LAWRENCE
LIVERMORE
NATIONAL
LABORATORY

UCRL-JRNL-224264

Interaction of Nocturnal Low-Level Jets with Urban Geometries as seen in Joint URBAN 2003 Data

J. K.Lundquist, J. D.Mirocha

September 7, 2006

Journal of Applied Meteorology and Climatology

Interaction of Nocturnal Low-Level Jets with Urban Geometries as seen in Joint URBAN 2003 Data

Julie K. Lundquist and Jeffrey D. Mirocha

Lawrence Livermore National Laboratory, Livermore, California 94551, USA

Submitted to the *Journal of Applied Meteorology*

September 11, 2006

Revised manuscript submitted May 16, 2007

Corresponding author address: J. K. Lundquist, Lawrence Livermore National Laboratory, P.O. Box 808, L-103, Livermore, CA 94551, Phone: (925) 422-1805, Fax: (925) 422-5844, E-mail: LUNDQUIST1@LLNL.GOV

Abstract.

As accurate modeling of atmospheric flows in urban environments requires sophisticated representation of complex urban geometries, much work has been devoted to treatment of the urban surface. However, the importance of the larger-scale flow impinging upon the urban complex to the flow, transport and dispersion within it and downwind has received less attention. Building-resolving computational fluid dynamics (CFD) models are commonly employed to investigate interactions between the flow and three-dimensional structures comprising the urban environment, however such models are typically forced with simplified boundary conditions that fail to include important regional-scale phenomena that can strongly influence the flow within the urban complex and downwind. This paper investigates the interaction of an important and frequently occurring regional-scale phenomenon, the nocturnal low-level jet (LLJ), with urban-scale turbulence and dispersion in Oklahoma City using data from the Joint URBAN 2003 (JU2003) field experiment. Two simulations of nocturnal tracer release experiments from JU2003 using Lawrence Livermore National laboratory's FEM3MP CFD model yield differing levels of agreement with the observations in wind speed, turbulence kinetic energy (TKE) and concentration profiles in the urban wake, approximately 750m downwind of the central business district. Profiles of several observed turbulence parameters at this location indicate characteristics of both bottom-up and top-down boundary layers during each of the experiments. These data are consistent with turbulence production due to at least two sources, the complex flow structures of the urban area and the region of strong vertical wind shear occurring beneath the LLJs present each night. While strong LLJs occurred each night, their structures varied considerably, resulting in significant differences in the magnitudes of the turbulence parameters observed during the two experiments. As FEM3MP was forced only with an upwind velocity profile that did not adequately represent the LLJ, the downward propagation of TKE observed

during the experiments was absent from the simulations. As such, the differing levels of agreement between the simulations and observations during the two experiments can, in part, be explained by their exclusion of this important larger-scale influence. We demonstrate the ability of the Weather Research and Forecast Model (WRF) to simulate accurate velocity fields during each night, and identify the use of regional-scale simulation data as a promising approach for representing the effects of important regional-scale phenomena such as the LLJ, on urban-scale simulations.

1. Introduction

The nocturnal low-level jet (LLJ) is a well-documented phenomenon which occurs frequently in many regions around the world. The LLJ has been studied in great detail in the southern Great Plains of the United States (Bonner 1968, Whiteman et al. 1997, Higgins et al. 1997, Banta et al. 2002, Song et al. 2005). These studies indicate the LLJ plays an important role in the transport of moisture, momentum, and air pollutants. In the canonical case first described by Blackadar (1957), the nocturnal LLJ forms following the attenuation of convective turbulent stresses from their afternoon maximum, allowing nighttime winds above a stable boundary layer to accelerate to supergeostrophic wind speeds. Additional mechanisms, such as baroclinicity due to sloping terrain (Holton 1967), can enhance jet accelerations. In situations with surface winds of less than 5 m s^{-1}, wind speeds at altitudes of 100m due to the nocturnal LLJ can be greater than 20 m s^{-1}. The turbulence generated by the strong wind shear beneath the jet can induce nocturnal mixing events and enhance surface-atmosphere exchange, thereby influencing the dispersion of hazardous materials near the surface in a manner consistent with the paradigm of top-down boundary layer development (Mahrt 1999).

In urban areas, the complicated atmospheric dispersion of hazardous materials is often simulated using high-resolution, building-resolving computational fluid dynamics (CFD) models such as Lawrence Livermore National Laboratory's FEM3MP model. These models focus on simulating the contributions of surface-based forcing to boundary-layer turbulence. Because resolving the effects of individual buildings demands grid cells on the order of 3m or lower, typical domains are on the order of 1 km x 1 km x 400m. Furthermore, such simulations are often driven by boundary conditions described only by an upwind profile, and boundary conditions at the top of the model domain often forbid vertical transport of momentum from

outside the simulation domain. Therefore, turbulence generated by LLJs or other mesoscale phenomena is not represented in these simulations. The inclusion of the effects of such phenomena in building-scale simulations requires coupling between CFD models and mesoscale models, which is an active area of research (Chan 2004, Chan and Leach 2004, Coirier et al. 2005, Pullen et al. 2005, Tewari et al. 2005). The consequences of including or excluding mesoscale effects remain undetermined and probably vary from case to case, but are likely to be very important in many situations.

Given the prevalence of the LLJ in the Southern Great Plains and the sound physical justification for including its effects in simulations of dispersion in the urban boundary layer, success of simulations excluding the effects of the LLJ in regions favoring its development would be surprising. A rich dataset is available for testing such urban boundary layer dispersion simulations, in the archives of the Joint URBAN 2003 (JU2003) tracer experiment, which was based in the Oklahoma City area. Despite the exclusion of mesoscale phenomena like the LLJ, FEM3MP simulations of the first release of JU2003 Intensive Observing Period (IOP) 9 agree well with observations of near-field winds and concentrations and of turbulence profiles in the urban wake region (Chan and Lundquist, 2005; Lundquist and Chan, 2005). However, simulations of another JU2003 release, the first release of IOP 8, show poor agreement in the urban wake region (Lundquist and Chan, 2007) although both nights exhibit LLJs and simulations on both night perform similarly well in the urban corridor region. This disparity motivates further investigation into the significance of mesoscale phenomena like the LLJ to urban transport and dispersion.

The present study is based on data from the JU2003 experiment, summarized in Section 2. Section 3 presents data describing the frequency and intensity of LLJs observed throughout the

JU2003 experiment, while Section 4 examines surface-layer forcing potentially induced by LLJs throughout the JU2003 experiment. As CFD models are rarely driven with mesoscale model input that would accommodate phenomena like the nocturnal LLJ and its effects, we look specifically for indications of top-down boundary layer development that would undermine the performance of CFD models driven without mesoscale forcing. Finally, Section 5 explores in detail IOPs 8 and 9, two nocturnal tracer releases which exhibit different jet behavior and jet effects on the surface layer. In addition to analysis of the field observations of jet behavior and surface-layer turbulent structure, mesoscale model simulations of the jets are presented; even these coarse simulations illustrate the possible effects of jets on surface-layer transport and dispersion.

2. The Joint URBAN 2003 field study

To provide quality-assured, high-resolution meteorological and tracer data sets for the evaluation and validation of indoor infiltration and outdoor urban dispersion models, the U.S. Department of Homeland Security and Department of Defense – Defense Threat Reduction Agency (DTRA) co-sponsored a series of dispersion experiments, named Joint URBAN 2003, in Oklahoma City (OKC), Oklahoma, during July 2003 (Allwine et al., 2004). These experiments provide a comprehensive field data set for the evaluation of CFD and other dispersion models.

The Joint URBAN 2003 (JU2003) experiment consisted of ten IOPs throughout late June and July of 2003. Six of the IOPs consisted of continuous and instantaneous daytime releases of sulfur hexafluoride tracer (SF_6) gas. Four of the IOPs (IOPs 6-10) occurred overnight. In addition to the tracer releases in the downtown Oklahoma City area, JU2003 participants collected extensive meteorological data characterizing the urban environment on the microscale (individual street canyons) and mesoscale. The present study considers the mesoscale properties

of the LLJ using data from one of three boundary-layer wind profilers that were deployed in the Oklahoma City region. This profiler, operated and maintained by Pacific Northwest National Lab (PNNL), was located about 2 km SSW of the downtown area. It operated with a vertical resolution of approximately 55m.

The mesoscale LLJ dataset has been constructed from 915 MHz boundary-layer wind profiler data collected by PNNL, archived at the JU2003 web archive, **http://ju2003-dpg.dpg.army.mil**, access to which may be requested via the website. The dataset extends from Julian Day (JD) 181 to 212 (30 June to 31 July). The dataset has been treated by PNNL with the NCAR Improved Moments Algorithm (NIMA) (Morse et al., 2002) to reduce or eliminate contamination of the wind speed data due to clutter or non-atmospheric interference. Nights corresponding to JD181 and 212 were eliminated from consideration due to missing data. Julian Days 202, 203, and 211 exhibited characteristics of frontal passages or other significant wind direction rotation overnight, and were thus not considered. The total boundary-layer wind profiler dataset thus consisted of twenty-seven nights from JD182 to JD 210, excluding JD 202 and 203. Data below 300m are not available because of noise in the radar signal due to ground clutter. This limitation restricts our ability to document the underside of the jet, but the analysis of Song et al. (2005) indicates that southerly jets in the Great Plains frequently exhibit a maximum wind speed at 350m, within the reach of this dataset.

To explore the microscale variability of the LLJ and its effect on turbulent mixing events, we use mean and fluctuating velocity and virtual temperature measurements from the Lawrence Livermore National Laboratory (LLNL) crane pseudo-tower, which was located approximately 750m NNW of the downtown area, often in the urban wake region (Lundquist et al., 2004). Eight sonic anemometers were mounted along this pseudo-tower, from 8-84m above the surface. We

also utilize observations of atmospheric sulfur hexafluoride concentrations from seven levels along the crane pseudo-tower; these observations were collected by a team from Washington State University.

Turbulence statistics presented here are calculated over 30-minute intervals; similarly, SF6 concentrations are presented as 30-minute averages.

3. Occurrences of LLJs during Joint URBAN 2003

Observations of wind speed and wind direction obtained from the PNNL 915 MHz boundary-layer wind profiler, located south of the Oklahoma City central business district, indicate the regular appearance of the LLJ during July 2003. We apply the minimum criteria used in other climatological studies of LLJs, that is that during the night, a maximum wind speed is found in a profile that surpasses a threshold of 10 m s^{-1} (category LLJ-0 in Whiteman et al. 1997 and Song et al. 2005, for example), with a decrease above the wind speed maximum of at least 5 m s^{-1}. We find that on each night examined here that includes profiles consistent with this LLJ criteria, the wind speed profile in the lowest 1000m accelerates after sunset, attaining a maximum wind speed typically between 700 and 1000 UTC (200 and 500 LT). Of the twenty-seven nights examined, only four nights (JDs 182, 192, 193, and 204) do not exhibit wind profiles consistent with those of LLJs. The twenty-three LLJ nights are not subdivided into categories as in Whiteman et al. (1997) and Song et al. (2005) because of the small number of nights examined.

3.1. Summary of JU2003 LLJ Characteristics

Climatological studies of LLJs traditionally categorize jets by their maximum overnight wind speed (Bonner, 1968, Mitchell et al., 1995, Whiteman et al., 1997, Song et al., 2005). The twenty-three LLJs observed during the JU2003 program exhibited maximum wind speeds

between 12 and 21 m s^{-1} (see Figure 1a). The degree of acceleration responsible for the development of the jet can be seen by inspecting "initial" wind speeds, or wind speeds at jet nose level at the beginning of the night, before the nocturnal accelerations presumed to generate LLJs occur. The distribution of these "initial" winds is shown in Figure 1b, while the distribution of the difference between the "initial" winds and the jet winds is shown in Figure 1c. In most cases, winds at jet nose level increase by at least 8 m s^{-1}, and in one case by 14 m s^{-1}.

The JU2003 jets were typically very low, as seen in Figure 1d: nearly half of the LLJs observed occur at the lowest three levels observable with the PNNL boundary-layer wind profiler. This result is consistent with that of Song et al. (2005), who survey six years of Southern Great Plains LLJs, not including the month of July 2003 examined here, using a similar instrument at a location in southern Kansas. Their analysis of data from 1997-2002 shows that the most common jet altitudes are at ~350m for southerly LLJs.

Most of the JU2003 LLJs are southerly or southwesterly jets, as seen in Figure 1e. This result is also consistent with that of Song et al. (2005), who find the dominant jet direction from 1997-2002 to be from the southwest. Some rotation of the jet nose overnight is seen, while the jet accelerates, but this rotation is typically less than 40 degrees (distribution not shown). Not all JU2003 LLJs decelerate over the course of the night. As shown in Figure 1f, 5 of the 23 LLJs achieve maximum wind speed in the last hour of the night, 1100-1200 UTC.

The degree of acceleration and the amount of overnight rotation associated with the LLJ has implications for the LLJ's effect on surface-layer turbulence and mixing. Strong shear on the underside of the jet produces intermittent and sometimes strong turbulent mixing that can propagate downward, perhaps even to the surface (Blumen et al., 2001). Smedman et al. (1993) have shown that turbulent kinetic energy (TKE) within the nose (level of maximum wind speed)

and below the nose of a LLJ scales as a function of distance from the core of the jet. Detailed quantification of the TKE within the nose of JU2003 LLJs is not available from the profiler data examined here. (High-resolution turbulence data may be available from the lidar datasets collected by Arizona State University and the Army Research Lab during JU2003 (Wang et al., 2006). Such data may provide insights into these LLJs in the same sense that Doppler lidar provided insights in the LLJ study of Banta et al. (2002).)

4. Surface-based observations

The transport of turbulent kinetic energy from the jet down to the surface has been regularly observed in jets, as in Mahrt and Vickers (2002). The LLNL crane pseudo-tower microscale dataset, described above, provides high-resolution wind speed observations necessary for calculation of variances, TKE, and the local rates of shear production, buoyant production, and local dissipation of TKE. The crane data have been tilt-corrected using the method of Wilczak, Oncley, and Stage (2001) lending credibility to calculation of vertical fluxes in particular. These observations near the surface and in the wake of the urban area indicate that observed turbulence is not generated exclusively locally by building-induced turbulence in the urban area but is also transported from aloft, likely from a mesoscale phenomenon like the LLJ.

Turbulent quantities, calculated over 30-minute intervals and averaged over all twenty-three LLJ nights (0030 UTC to 1200 UTC) are presented here in Figure 3. In aggregate, ignoring the considerable variability that occurs over the course of individual nights, these profiles suggest that the nocturnal boundary layers observed at the crane site, downwind of the OKC urban area are not simply top-down or bottom-up boundary layers. Rather, they exhibit characteristics both of top-down boundary layers, in which turbulence is generated aloft and transported down, as well as surface-forced boundary layers, in which turbulence is generated within the surface layer

(and in the case of urban areas, passage through urban structures). Figure 2 depicts a conceptual picture of how interactions, between turbulence generated aloft by LLJs and turbulence generated by flow through the urban matrix of buildings, can result in increased near-surface TKE and vertical mixing within the urban area and downwind.

The averaged profile of vertical velocity with negative values indicating downward motion is seen in Figure 3a, in which negative values indicate downward motion. Considerable subsiding vertical motions are seen at the upper levels of the crane. These values are about three times larger than those observed in large-scale descriptions of boundary-layer subsidence (Yi et al., 2001), and may be representative rather of either forcing from the LLJ or motions characteristic of the urban wake region.

A typical characterization of the upside-down boundary layer is that the standard deviation of vertical velocity is larger at higher levels than at lower levels, as discussed in Mahrt and Vickers (2002). As shown in Figure 3b, values of this parameter at the top of the crane are 30% higher than closer to the surface, again suggesting top-down forcing of the boundary layer, consistent with the hypothesis that shear from the underside of a LLJ generates turbulence that is transported down into the boundary layer. Hence these boundary layers exhibit some characteristics of upside-down boundary layers.

The profile of TKE is shown in Figure 3c. Although the mean profile clearly indicates higher values of TKE aloft, as compared to values close to the surface, the range of TKE values over these 23 nights is large, with a standard deviation of 14% at the 8m level and 33% at the 83m level. Distinguishing the portion of the TKE due to the turbulent mixing generated by flow through the urban area immediately upwind of the observing tower from the portion induced by

mesoscale effects such as the LLJ is difficult, and will be addressed below in conjuction with analysis of the modeling studies.

It has been suggested (Mahrt and Vickers, 2002, and Banta et al., 2006) that the sign of the vertical transport of vertical velocity variance $\overline{w'^3}$, which appears in Figure 3d, indicates the direction of turbulent transport. The data shown in Figure 3d then illustrate upward transport of the urban-induced turbulence, as opposed to the downward motions implied by the data in Figure 3a-c. Similarly, the vertical transport of TKE, or $\overline{w'e}$, shown in Figure 3e, also indicates upward transport of TKE.

However, when the vertical velocity variance is normalized by the standard deviation of the vertical velocity, the result is the skewness ($\overline{w'^3}/\sigma_w^3$), which is conventionally considered a measure of the asymmetry of the probability density function of the vertical velocity fluctuations. Following Tennekes and Lumley (1972, p.200), we interpret the sign of the skewness to indicate the qualitative structure of the flow rather than strictly identifying the direction of the transport. As in Moeng and Rotunna (1990), positive skewness indicates strong short-duration updrafts superimposed on a mean field of weaker downward motions. Higher values of skewness are due to more asymmetry, or fewer strong short-duration updrafts. We propose that the profile of $\overline{w'^3}$ shown in Figure 3d and the skewness profile shown in Figure 3f represent the interaction of the urban-generated turbulence (in the form of strong short-duration updrafts) with low-level jet generated turbulence representing weaker continuous downward motions. When the skewness is small, as in the lower portions of the tower, there is a more equitable mix between the two influences. Higher on the tower, the skewness is larger, indicating that there are fewer strong short-duration updrafts able to penetrate the continuous downward motions, and the jet's downwelling influence is stronger.

In summary, the averaged microscale observations from the crane pseudo-tower on the nights with LLJ activity indicate the complex interplay between the urban-generated turbulence and the turbulence generated aloft from the LLJ. We find strong short-duration updrafts due to urban-generated turbulence superimposed on a mean field of weaker downward transport of momentum. Individual nights exhibit variability in the mean values of these turbulent quantities as well as their evolution through the overnight hours. Variability can be induced by several factors, including the magnitude of the shear associated with the LLJ. In the following section, we contrast the two IOPs, each featuring similar LLJs but with different turbulence characteristics. The disparate success of these simulations is consistent with variability in the mesoscale flow and LLJs that is identified in measurements and reproduced during simulations using the mesoscale model, WRF.

5. Comparison of IOPs 8 and 9

Previous work has shown that a CFD simulation of IOP 9 (JD 208) shows very good agreement with the wind speed and turbulence quantities measured at the crane pseudo-tower, in the urban wake region, even though that simulation excludes the possibility of the vertical transport of TKE (Chan and Lundquist 2005). In contrast, Lundquist and Chan (2007) present a simulation of IOP 8 (JD206), which indicates that a CFD simulation generates much less turbulence at the crane site than is observed and that the deviation is larger at higher levels on the crane, indicating possible mesoscale influences like the LLJ. These two cases are discussed in more detail here to explore the extent to which shear generated by the LLJ induces vertical transport of TKE during IOP8 and not in IOP9, thus partially explaining the success of CFD with IOP9 and not with IOP8.

Section 5.1 summarizes the results of the CFD simulations. Section 5.2 discusses the LLJs on these two nights as observed with boundary-layer wind profilers, while Section 5.3 discusses the surface-layer turbulence variability on these two nights. The relationship between the mesoscale jets and boundary-layer turbulence is underscored using mesoscale numerical weather prediction simulations in Section 5.4.

5.1. CFD simulations of IOP8 and IOP9

Figure 4 illustrates the performance of the FEM3MP simulations of IOP8 and IOP9, previously presented in Chan and Lundquist (2005) and Lundquist and Chan (2007). Herein, we highlight certain aspects of the model performance and also provide a comparison to the crane tracer concentration profiles to emphasize the poor performance on IOP8 as compared to the good performance for IOP9.

Standard methods for establishing inflow conditions were used for both simulations. Logarithmic wind profiles constituted the inflow boundary conditions for both IOP 8 and 9. In both cases, the wind speed and direction were estimated by averaging the data of PNNL sodar (located ~ 2 km SSW of downtown OKC) at the 50 m level from 0400 to 0430 UTC, the same time of the simulated releases. The roughness length scale was assumed to be 0.3 m. For IOP 8, the estimated wind speed at 50 m is 5.0 m s^{-1} and the wind direction is 155 degrees. For IOP 9, the estimated wind speed is 5.8 m s^{-1} and the wind direction is 167 degrees.

As shown in Figure 4(b,d, and f), the simulation results for IOP9 agree well with observations. The wind speed profile (Figure 4b) has a slightly different shape, but the same averaged value. The TKE profile (Figure 4d) agrees very well, and tracer concentrations (Figure 4f) predicted by FEM3MP are within 20% of the observed values. In summary, FEM3MP, which assumes a neutrally-buoyant atmosphere and explicitly resolves building-induced turbulence,

seems to capture the dominant physical influences on the urban atmosphere at the time of IOP9 in the urban wake region. On the other hand, the comparison between FEM3MP predictions and observations at the crane location for IOP8 indicate that other physical processes, not accounted for by FEM3MP, dominate the flow. FEM3MP underpredicts momentum as reflected in the wind speed profile (Figure 4a). The observed TKE profile (Figure 4c) also indicates another source of TKE other than that simulated by FEM3MP. Finally, FEM3MP overpredicts tracer concentrations by a factor of 2 (Figure 4e), which is consistent with the underprediction of turbulent mixing. In summary, FEM3MP, at least as initialized with a logarithmic inflow boundary condition and no nesting with a mesoscale model that could account for influences outside of the FEM3MP domain, cannot account for all the physical processes that affect the atmosphere during IOP8.

5.2. LLJs on IOP8 and IOP9

Both of the nights simulated with the FEM3MP CFD capability exhibit LLJ structure in the mean winds as observed with the PNNL boundary-layer wind profiler, although those LLJs are not represented in the CFD simulations. The time evolution of their wind speed profiles, shown in Figure 5a (IOP8, JD206) and Figure 5b (IOP9, JD208), are similar, with the jets attaining wind speed maxima greater than 17 m s^{-1} relatively late in the night (1130 UTC at 500m for IOP8; 1030 UTC at 500m for IOP9). (Most of the JU2003 LLJs attained their wind speed maxima between 0700 and 1200 UTC, as shown in Figure 1f.) The evolution of the jets between 0200 and 0700 UTC do vary: the IOP8 (JD206) jet exhibits a continuous increase of wind speed, while the IOP9 (JD208) jet actually decelerates from 0200 to 0500 UTC, accelerating again by 0600 UTC and throughout the rest of the night. The jets' accelerations are similar; the change in wind speed from the beginning of the night to the jet max was approximately 11 m s^{-1} for IOP8

and 10 m s^{-1} for IOP9. The nose of the IOP9 (JD208) jet also rises after 0800 UTC. Finally, wind speeds above 1500m are higher for the IOP8 (JD206) jet.

More obvious differences are seen in the wind direction profiles of these two jets in the lowest 1000m . Although the wind speeds in the lowest levels are very similar, the IOP8 (JD206) jet rotates only slightly (14 degrees) over the course of the night (Figure 5c), while the IOP9 (JD208) jet rotates considerably in a manner consistent with inertial forcing (Figure 5d), from 169 degrees to 230 degrees, for a rotation of approximately 60 degrees. These differences in the overnight rotation of low-level winds could be due to large-scale effects also seen in the wind speed and direction profiles above 1000m. The large variability aloft during IOP8 (JD206) suggests the possibility of additional mesoscale effects on the flow beyond those associated with the low-level forcing by the LLJ. Such mesoscale effects are difficult to characterize or include in CFD simulations.

The direction of the rotation of the both jets, as seen in their hodographs from the 632m level (Figure 5e, f) is consistent with Blackadar's hypothesis that the inertial oscillation contributes to the jet maxima. He hypothesized that the inertial oscillation generated by the evening's release of convectively-driven turbulence stresses causes winds in the residual boundary layer to become supergeostrophic. However, identifying an exact inertial oscillation superimposed on an evolving geostrophic wind field is quite difficult (Lundquist, 2003), particularly at this latitude, as confirmed in the LLJ modeling study of Jiang et al. (2007).

5.3. Crane observations of downward propagation of TKE during IOPs 8 and 9

An intercomparison of turbulent quantities at the crane pseudo-tower clearly indicates differences between the two nights, and implicates downward transport of momentum and

turbulence as one factor in the poor agreement between observations and CFD simulations for IOP8 (JD206).

As discussed above, the turbulence observations at the crane location indicate a complex interplay between upward urban-induced turbulence and downward motions arising from the LLJ. The skewness, or measure of the asymmetry of the vertical motions, can be interpreted as an indication of how high the urban-induced turbulent motions persist. (Recall that in large-eddy simulations of bottom-heated convective boundary layers, skewness is small at the surface, asymptotes to a constant value through the bulk of the boundary layer, and increases substantially near the top of the boundary layer where few upward motions penetrate, as seen in Moeng and Rotunno (1990), Fig. 7.)

It is important to remember that skewness is larger and more positive when there are fewer strong updrafts against a background of downward motions induces by mesoscale activity like the LLJ. The time-height cross-section of skewness during IOP8 (JD206) (Figure 6a) indicates intermittent periods of increased skewness, especially at the upper levels and sometimes extending down to the 20m level. Although these intermittent bursts are seen throughout the night, starting at 0200 UTC, the activity is particularly pronounced during the time period simulated in Chan and Lundquist (2006), 0400-0430 UTC. Therefore, we interpret these "bursts" in skewness as indicative of time periods when few urban vortices can penetrate the background of stronger mesoscale downward motions. Most urban upward motions lose their identity when mixing with the background turbulence, and skewness increases. Because the CFD simulations lack any mesoscale downward transport, this interaction cannot be represented in those simulations. Without turbulence observations between the top of the crane (83m) and the nose of the jet (500m, as seen in Figure 5a), it is not possible to precisely quantify the downward

transport or attribute it directly to the LLJ, however, both the measurements we do have and physical reasoning support this interpretation.

In comparison, IOP9 exhibits reduced variability and therefore a diminished mesoscale role, as seen in Figure 6b. Intermittent bursts of activity are seen only early in the night, around 0100 UTC, beginning again after 0700 UTC. The time period of 0400-0430 UTC (simulated in Chan and Lundquist (2005)) is particularly quiescent.

Other turbulent quantities support the conclusion that IOP8 proved to be difficult to simulate due to more interplay between the mesoscale and the urbanscale as seen in larger vertical velocity fluctuations (Figure 6c and Figure 6d) and slightly higher values of TKE (Figure 6e and Figure 6f). The standard deviation of vertical velocity, σ_w, exhibits high values (greater than 1.0 m s^{-1}) soon after 0200 UTC during IOP8 (Figure 6c), while during IOP9 (Figure 6d), high values do not occur until after 0530 UTC and do not persist through the night. Similarly, turbulent kinetic energy values exceed 3.0 m^2 s^{-2} occur soon after 0400 UTC and persist through most of IOP8 (Figure 6e). During IOP9 (Figure 6f), a brief burst of TKE greater than 3.0 m^2 s^{-2} occurs around 0200 UTC but these high values do not persist through most of the night.

5.4. Mesoscale model simulations of JD206 and JD208

We attribute the difference between IOP8 and IOP9 to the role of mesoscale forcing, via the LLJ. The nocturnal LLJ and its role in the evolution of the boundary-layer TKE field during the nights of IOPs 8 and 9 are investigated further using the Weather Research and Forecasting (WRF) model (http://www.wrf-model.org). The simulations are initialized at 0300 UTC (0800 CDT) on the day preceding each IOP to allow ample time for spin-up (26 hours) prior to the convective portion of the diurnal cycle, the inclusion of which is crucial to the subsequent development of the LLJ.

The WRF model domain consists of 72 gridpoints spaced 4km apart in each horizontal direction, and 62 gridpoints in the vertical. The lowest gridpoint is approximately 15m above the surface, with 14-15 height levels within the lowest 1000m. Initial and boundary conditions are obtained from National Centers for Environmental Prediction (NCEP) North American Regional Reanalysis (NARR) data, which provides atmospheric fields from the ETA 32km/45-layer model on the ETA 212 (32km) grid at 29 pressure levels every three hours. The simulations utilize the 2.5-order prognostic TKE parameterization of Janjić (2002) for boundary-layer physics.

Figure 7 shows the simulated wind speed and TKE fields during the nights of IOPs 8 and 9, with time-height sections during 13-hour periods containing each of the IOPs in the upper panels, and the profiles at the time of the IOPs below. The left panels depict the acceleration of the low-level winds beginning a few hours after the diurnal TKE maximum (occurring around 2100 UTC (1600 CDT), not shown). The time-height sections (right panels) of TKE show that, during both nights, TKE reaches a minimum value just a few hours after sunset (0000 UTC or 1900 CDT), after which it begins to increase as a result of increasing shear in the presence of accelerating winds aloft. However, the behavior of the low-level wind and TKE fields during the two nights diverges during the early morning hours. During the early morning of IOP8, the jet maximum wind speed increases, decreases, and increases again while the nose of the jet remains at a constant altitude. After 0800 UTC (0300 CDT), the jet maximum persists at a constant wind speed for several hours. During IOP9, the jet maximum wind speed increases until 0700 UTC (0200 CDT), after which it decreases in a fashion typical of the classic LLJ described by Blackadar (1957).

The differences in the behavior of the LLJ during these two nights are reflected in the evolution of the TKE. During IOP8, TKE gradually increases throughout the early morning

hours in response to sustained low-level shear. IOP 8's higher levels of LLJ-induced TKE, particularly near the surface, are consistent with our hypothesis that LLJ-induced mesoscale turbulence exerts more of a role during IOP8, more actively suppressing the urban upwelling turbulence and increasing the skewness of the vertical velocity motions. In contrast, during IOP9, TKE increases for only a few hours before decreasing again following the weakening of the LLJ. Average TKE values are lower, indicating that the mesoscale effect is less significant during IOP9.

The behaviors of the LLJ and boundary-layer TKE during the simulations of each of these nights are consistent with trends in the observational data. The wind speeds measured by the PNNL wind profiler show increased hour-to-hour variability and lower sustained values during IOP 9 than during IOP 8. Both TKE and vertical velocity variance measured at the LLNL crane pseudo-tower likewise indicate weaker turbulence during IOP9 relative to higher values during IOP8.

The large values of vertical velocity skewness measured by the crane pseudo-tower during the nights of IOPs 8 (Figure 6a) and 9 (Figure 6b) are consistent with the hypothesis that IOP8 witnessed an more dynamic interplay between downward mesoscale motions, punctuated by brief strong updrafts due to urban effects. Such a pattern indicates the existence of an elevated source of TKE above the urban area, which is most likely the strong shear beneath the LLJ. During the night of IOP8, skewness (Figure 6a) attains a greater maximum value which persists for longer durations than during IOP9, indicating that strong large-scale forcing during the night of IOP8 maintains sufficient wind speeds for persistent TKE production and downward transport during the night of IOP8. During the night of IOP9, skewness (Figure 6b) shows a generally smaller peak value and longer periods of very small values, suggesting that the weaker large-

scale forcing during the night of IOP9 fails to generate or maintain wind speeds necessary for persistent TKE production, resulting in a more regular influence from the urban area and lower values of skewness.

These regional-scale WRF simulations capture the characteristics of the large-scale flow that impact low-level wind and TKE fields, as well as their variability from one night to the next. As both the observations and results of the CFD simulations show, in addition to representation of urban surface roughness effects, the downward transport of TKE from the LLJ toward the surface could be critical to successful modeling of flow and transport in the urban environment. Nesting a CFD model within a regional-scale model represents one possible approach to incorporating important regional-scale effects on flow, transport and dispersion in urban environments.

6. Summary and Conclusions

The phenomenon of the nocturnal LLJ appears regularly in the meteorological dataset collected in conjunction with the Joint URBAN 2003 tracer field experiment. Twenty-three of the twenty-seven nights examined show significant LLJs, often with accelerations overnight greater than 10 m s^{-1}. Consistent with previous studies in this region, most LLJs are southerly or southwesterly, with the maxima in wind speed occurring below 500m AGL.

Despite the prevalence of the LLJ and indications that LLJs can induce turbulent mixing events that propagate down to the surface, previous work has shown that a CFD simulation of IOP 9 (JD 208) shows very good agreement with the turbulence quantities measured at the crane pseudo-tower, even though that simulation excludes the possibility of the vertical motion due to mesoscale effects(Chan and Lundquist 2005, Lundquist and Chan 2005). However, Chan and

Lundquist (2006) present a simulation of IOP 8 (JD206), which indicates that a CFD simulation generates much less turbulence at the crane site than is observed, and that the deviation is larger at higher levels on the crane, indicating possible mesoscale influences like the LLJ. These two cases are presented to explore the extent to which shear generated by the LLJ induces vertical transport of TKE during IOP8 and not in IOP9, thus explaining the success of CFD with IOP9 and not with IOP8. Considerable activity is seen during IOP8, while relative quiescence occurs during the simulation period of IOP9.

Due to the important turbulent mixing events potentially induced by mesoscale phenomena such as the ubiquitous LLJ, high-resolution simulations of transport and dispersion in the urban environment should incorporate such mesoscale effects. Nesting such CFD simulations within a mesoscale model is one promising approach.

Acknowledgments. This work was performed under the auspices of the U.S. Department of Energy by the University of California, Lawrence Livermore National Laboratory under contract No. W-7405-Eng-48. UCRL-JRNL-224264. The WRF boundary conditions data were provided by the Data Support Section of the Scientific Computing Division at the National Center for Atmospheric Research (NCAR). NCAR is supported by grants from the National Science Foundation. The authors appreciate the data collection efforts of the other Joint URBAN 2003 participants, as well as scientific discussions with Stevens T. Chan, Branko Kosović, and Larry Mahrt. We also value the input from our three anonymous reviewers.

References

Allwine, K., and co-authors, 2004: Overview of Joint Urban 2003, AMS Annual Meeting, Seattle, WA, Jan. 11-15, 2004. Available at http://ams.confex.com/ams/84Annual/techprogram/paper_74349.htm

Banta, R. M., R. K. Newsom, J. K. Lundquist, Y. L. Pichugina, R. L. Coulter, and L. Mahrt, 2002: Nocturnal low-level jet characteristics over Kansas during CASES-99. *Bound.-Layer Meteor.,* **105**, 221-252.

Blackadar, A.K., 1957: Boundary layer wind maxima and their significance for the growth of nocturnal inversions. *Bull. Amer. Meteorol. Soc.*, **38**, 283-290.

Blumen, W., R. Banta, S. P. Burns, D. C. Fritts, R. Newsom, G. S. Poulos, and J. Sun, 2001: Turbulence statistics of a Kelvin-Helmholtz billow event observed in the night-time boundary layer during the Cooperative Atmosphere-Surface Exchange Study field program. *Dyn. Atmos. Oceans***.,** 34, 180-204.

Bonner, W.D., 1968: Climatology of the low level jet. *Mon. Weath. Rev.*, **96**, 833-850.

Chan, S., 2004: Incorporation of Large Scale Forcing into a Building Scale CFD Model. Workshop on Merging Mesoscale and CFD Modeling Capabilities, 2004 AMS Annual Meeting, Seattle, WA, 11 January 2004.

Chan, S., and M. Leach, 2004: Large Eddy Simulation of an URBAN 2000 Experiment with Various Time-dependent Forcing. 5th Symposium on the Urban Environment, Vancouver, Canada, Aug. 23-27, 2004.

Chan, S. and J.K. Lundquist, 2005: A Verification of FEM3MP Predictions Against Field Data from Two Releases of the Joint URBAN 2003 Experiment. 9th GMU Conference on Atmospheric Transport and Dispersion Modeling, Fairfax, VA, July 18-20, 2005.

Chan, S. and J.K. Lundquist, 2006: A Study of Stability Conditions in an Urban Area. AMS 6th Symposium on the Urban Environment, Atlanta, Georgia, Jan 29 – Feb 2, 2006.

Coirier, W.J., S.X. Kim, F. Chen, and M. Tewari, 2005: Demonstration and Evaluation of Coupled Mesoscale (WRF) and Urban-scale (FRD-Urban) Models. 9th GMU Conference on Atmospheric Transport and Dispersion Modeling, Fairfax, VA, July 18-20, 2005.

Higgins, R.W., Y. Yao, E.S. Yarosh, J.E. Janowiak, and K.C. Mo, 1997: Influences of the Great Plains low-level jet on summertime precipitation and moisture transport over the central United States. *J. Climate*, **10**, 481-507.

Holton, J. R., 1967: The diurnal boundary layer wind oscillation above sloping terrain. *Tellus*, **19**, 199-205.

Janjic, Z. I. 2002: Nonsingular Implementation of the Mellor-Yamada Level 2.5 Scheme in the NCEP Meso Model. *NCEP Office Note*, **No. 437**, 61 pp.

Jiang, X., N.-C. Lau, I. M. Held, and J. J. Ploshay, 2007: Mechanisms of the Great Plains Low-Level Jet as Simulatied in an AGCM. *J. Atmos. Sci.* **64**, 532-547.

Lundquist, J.K., 2003: Intermittent and Elliptical Inertial Oscillations in the Atmospheric Boundary Layer. *J. Atmos. Sci.*, **60**, 2661-2673.

Lundquist, J.K., J.H. Shinn, and F. Gouveia, 2004: Observations of Turbulent Kinetic Energy Dissipation Rate in the Urban Environment. AMS Symposium on Planning, Nowcasting, and Forecasting in the Urban Zone at the 84th Annual Meeting, Seattle, WA, Jan. 11-15, 2004.

Lundquist, J. K. and S. Chan, 2005: Analysis of Joint URBAN 2003 Wind and Turbulence Profiles and Comparison with FEM3MP Simulations. 9th GMU Conference on

Atmospheric Transport and Dispersion Modeling, Fairfax, VA, July 18-20, 2005. Available at https://narac.llnl.gov/documents.php

Lundquist, J. K., and S. T. Chan, 2007: Consequences of Urban Stability Conditions for Computational Fluid Dynamics Simulations of Urban Dispersion.Accepted to *J. Appl. Meteorol. Climatol.*

Mahrt, L., 1999: Stratified atmospheric boundary layers. *Bound.-Layer Meteor.*, **90**, 375-396.

Marht, L., and D. Vickers, 2002: Contrasting vertical structures of nocturnal boundary layers. *Bound.-Layer Meteor.*, **105**, 351-363.

Mellor, G. L., and T. Yamada, 1982: Development of a turbulence closure model for geophysical fluid problems. *Rev. Geophys. Space Phys.,* **20**, 851-875.

Mitchell, M.J., R.W. Arritt, and K. Labas, 1995: A Climatology of the Warm Season Great Plains Low-Level Jet Using Wind Profiler Observations. *Wea. Forecasting*, **10**, 576-691.

Moeng, C.-H. and R. Rotunno, 1990: Vertical-Velocity Skewness in the Buoyancy-Driven Boundary Layer. *J. Atmos. Sci.*, **47**, 1149-1162.

Morse, C.S., R.K. Goodrich, and L. B. Cornman, 2002: The NIMA method for improved moment estimation from Doppler spectra. *J. Atmos. Ocean. Tech.* **19**, 274-295.

Pullen, J., J. Boris, G. Patnaik, T. Young, and T. Holt, 2005: Linked Mesoscale-LES Contaminant Prediction for Manhattan. 9th GMU Conference on Atmospheric Transport and Dispersion Modeling, Fairfax, VA, July 18-20, 2005.

Smedman, A.-S., M. Tjernström, and U. Högström, 1993: Analysis of the Turbulent Structure of a Marine Low-Level Jet. *Bound.-Layer Meteor.*, **66**, 105-126.

Song, J. K. Liao, R. L. Coulter, and B. M. Lesht, 2005: Climatology of the low-level jet at the Southern Great Plains Atmospheric Boundary Layer Experiments site. *J. Appl. Meteorol.*, **44**, 1593-1606.

Tennekes, H. and J. L. Lumley, 1972. A First Course in Turbulence. The MIT Press. 300 pp.

Tewari, M., F. Chen, T. Warner, W.J. Coirier, and S. Kim, 2005: Application and Evaluation for the Coupled WRF-Noah-Urban Model for the complex Salt Lake City Urban Region. 9th GMU Conference on Atmospheric Transport and Dispersion Modeling, Fairfax, VA, July 18-20, 2005.

Wang, Y.. , C. Klipp, C. Williamson, G. Huynh, D. Garvey, S. Chang, 2006: An Investigation of Nocturnal low-level-jet generated gravity waves and turbulence over Oklahoma City during JU2003. AMS Annual Meeting, Atlanta, GA, Jan. 29 – Feb. 2, 2006. Available at http:// ams.confex.com/ams/pdfpapers/100877.pdf

Whiteman, C.D., X. Bian, and S. Zhong, 1997: Low-level jet climatology from enhanced rawindsonde observations at a site in the southern Great Plains. *J. Appl. Meteorol.*, **36**, 1363-1376.

Wilczak, J. M., S. P. Oncley, and S. A. Stage, 2001: Sonic anemometer tilt correction algorithms. *Bound.-Layer Meteorol.* **99**, 127-150.

Yi, C., K. J. Davis, B.W. Berger, and P.W. Bakwin, 2001: Long-Term Observations of the Dynamics of the Continental Planetary Boundary Layer. *J. Atmos. Sci.,* 58, 1288-1299.

List of Captions

Figure 1: Climatology of LLJs observed during JU2003: Distributions of a) maximum overnight wind speed (at nose of LLJ), b) wind speeds at 1930 Local Time (0030 UTC) at the altitude at which the jet nose forms, c) increase of wind speed over the night at the altitude of the LLJ, d) heights of the LLJ "nose", or wind speed maximum, e) wind directions at the LLJ "nose", or wind speed maximum, and f) UTC times of attainment of wind speed maxima.

Figure 2: Idealized nocturnal wind speed and resulting TKE profiles: a) near-surface TKE generation due to surface roughness b) is enhanced by the presence of urban structures. c) Shear and wave-induced TKE generation occurring in the upper ABL in the presence of the low level jet can propagate downward to augment near-surface TKE d) resulting in further TKE enhancement within urban environments, increased vertical mixing, and possibly a **significantly increased mixing height.**

Figure 3: Averaged profiles from 0030 UTC to 1200 UTC for the 23 LLJ nights of JU2003: a) vertical velocity, b) $\sigma\omega$, the standard deviation of vertical velocity, c) turbulent kinetic energy, d) vertical transport of vertical velocity, e) vertical transport of turbulent kinetic energy.

Figure 4: Comparison of CFD results at the crane location to observations: a) velocity profile for IOP8, b) velocity profile for IOP9, c) TKE profile for IOP8, d) TKE profile for IOP9, e) SF6 concentration profile for IOP8, f) SF6 concentration profile for IOP9. Note the good agreement for IOP9 (b,d,f) and the poor agreement for IOP8 (a,c,e).

Figure 5: The evolution of wind profiles every 30 minutes from 0030 UTC (black) to 1200 UTC (orange) on the nights of IOP8 (a,c,e) and IOP9 (b,d,f): a) wind speed for IOP8, b) wind speed for IOP9, c) wind direction for IOP8, d) wind direction for IOP9, e) hodograph from 630m level for IOP8, f) hodograph from 630m for IOP 9.

Figure 6: Time-height cross-sections from 0000 UTC to 1200 UTC on the nights of IOP8 (left panels a, c, e) and IOP9 (right panels b, d, f): a) skewness during IOP8, b) skewness during IOP9, c) $\sigma\omega$, the standard deviation of vertical velocity during IOP8, d) $\sigma\omega$, the standard deviation of vertical velocity during IOP9, e) TKE during IOP8, f) TKE during IOP9.

Figure 7: WRF simulations of the nights of IOPs 8 and 9. a) Time-height cross section of wind speed in the lowest 1000m from 0000 UTC to 1300 UTC on the night of IOP8. b) Time-height cross-section of turbulent kinetic energy in the lowest 1000m from 0000 UTC to 1300 UTC on the night of IOP8. c) As in a), but for IOP9. d) As in b), but for IOP9. e) Profiles of wind speed at the time of the CFD simulations, showing that the wind speed maximum for IOP 8 exceeds that of IOP9. f) Profiles of simulated TKE at the time of the CFD simulations, showing higher levels of TKE for IOP8 than for IOP9, but much smaller than observed or simulated by FEM3MP.

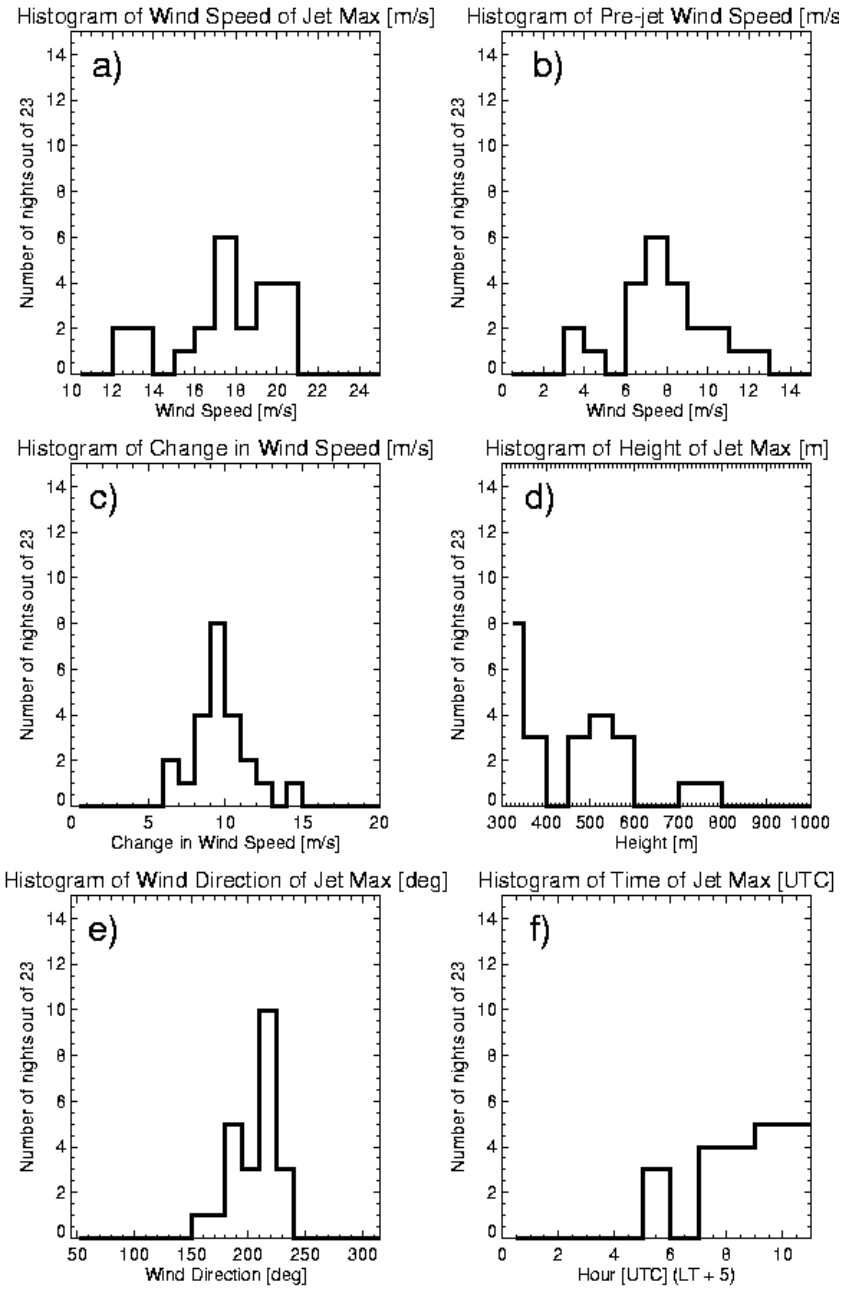

Figure 1: Climatology of LLJs observed during JU2003: Distributions of a) maximum overnight wind speed (at nose of LLJ), b) wind speeds at 1930 Local Time (0030 UTC) at the altitude at which the jet nose forms, c) increase of wind speed over the night at the altitude of the LLJ, d) heights of the LLJ "nose", or wind speed maximum, e) wind directions at the LLJ "nose", or wind speed maximum, and f) UTC times of attainment of wind speed maxima.

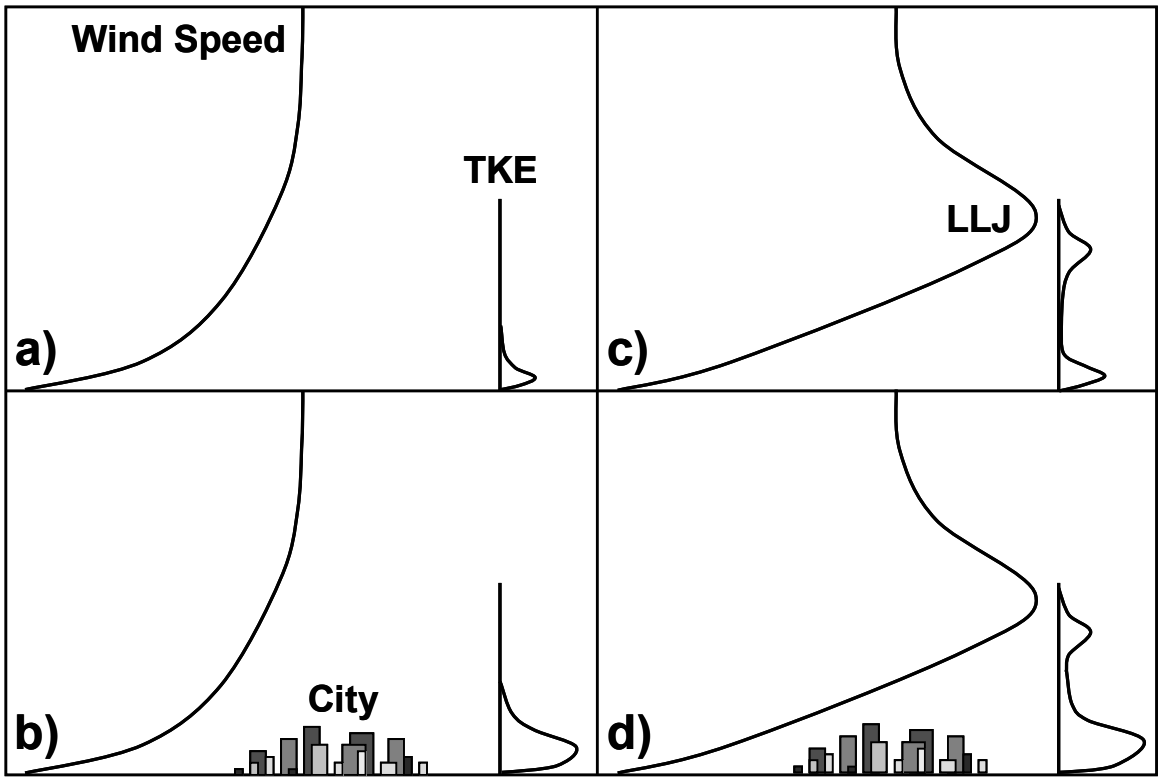

Figure 2: Idealized nocturnal wind speed and resulting TKE profiles: a) near-surface TKE generation due to surface roughness b) is enhanced by the presence of urban structures. c) Shear and wave-induced TKE generation occurring in the upper ABL in the presence of the low level jet can propagate downward to augment near-surface TKE d) resulting in further TKE enhancement within urban environments, increased vertical mixing, and possibly a significantly increased mixing height.

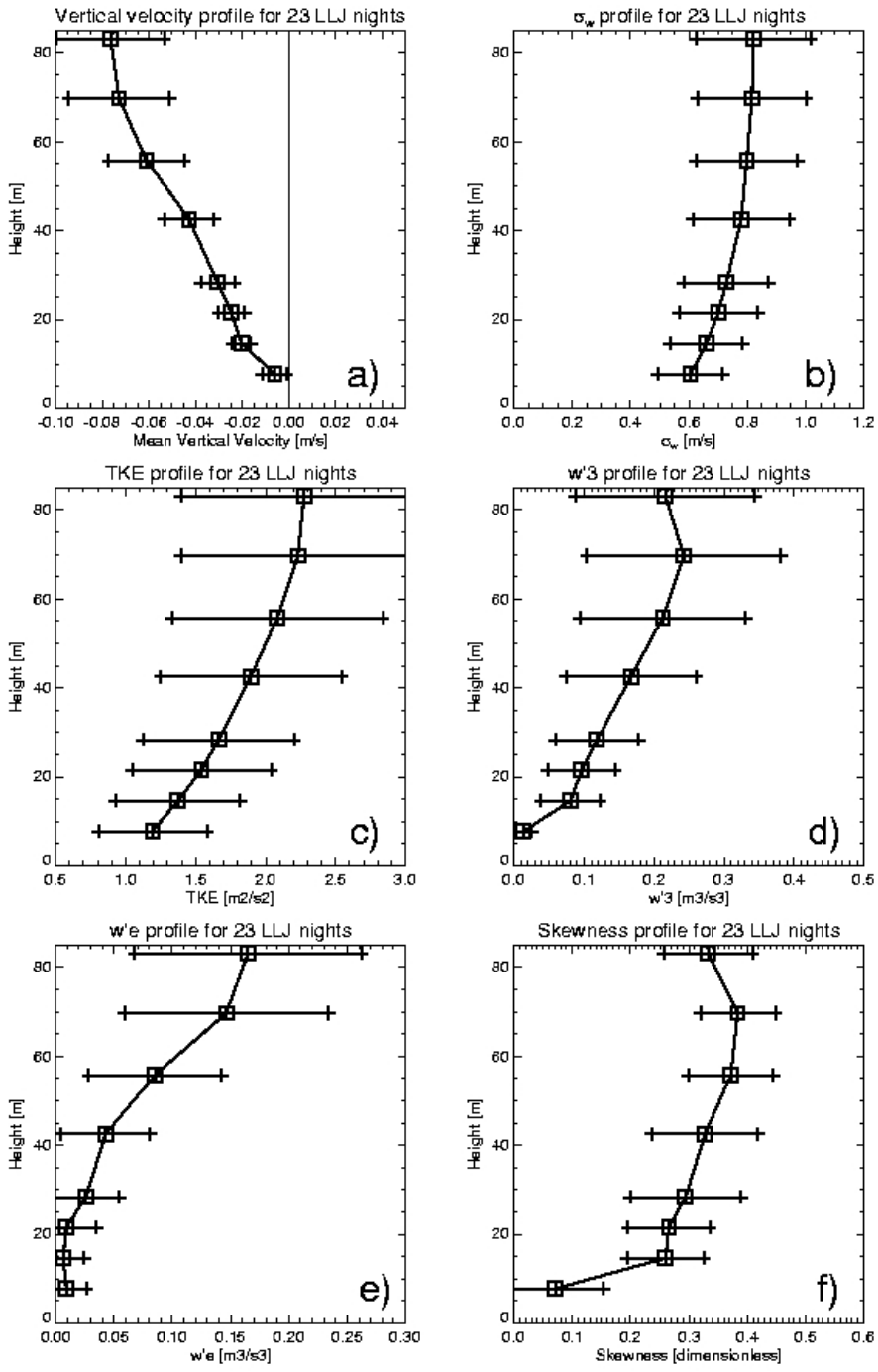

Figure 3: Averaged profiles from 0030 UTC to 1200 UTC for the 23 LLJ nights of JU2003: a) vertical velocity, b) σ_w, the standard deviation of vertical velocity, c) turbulent kinetic energy, d) vertical transport of vertical velocity, e) vertical transport of turbulent kinetic energy. Error bars indicate +/- one standard deviation.

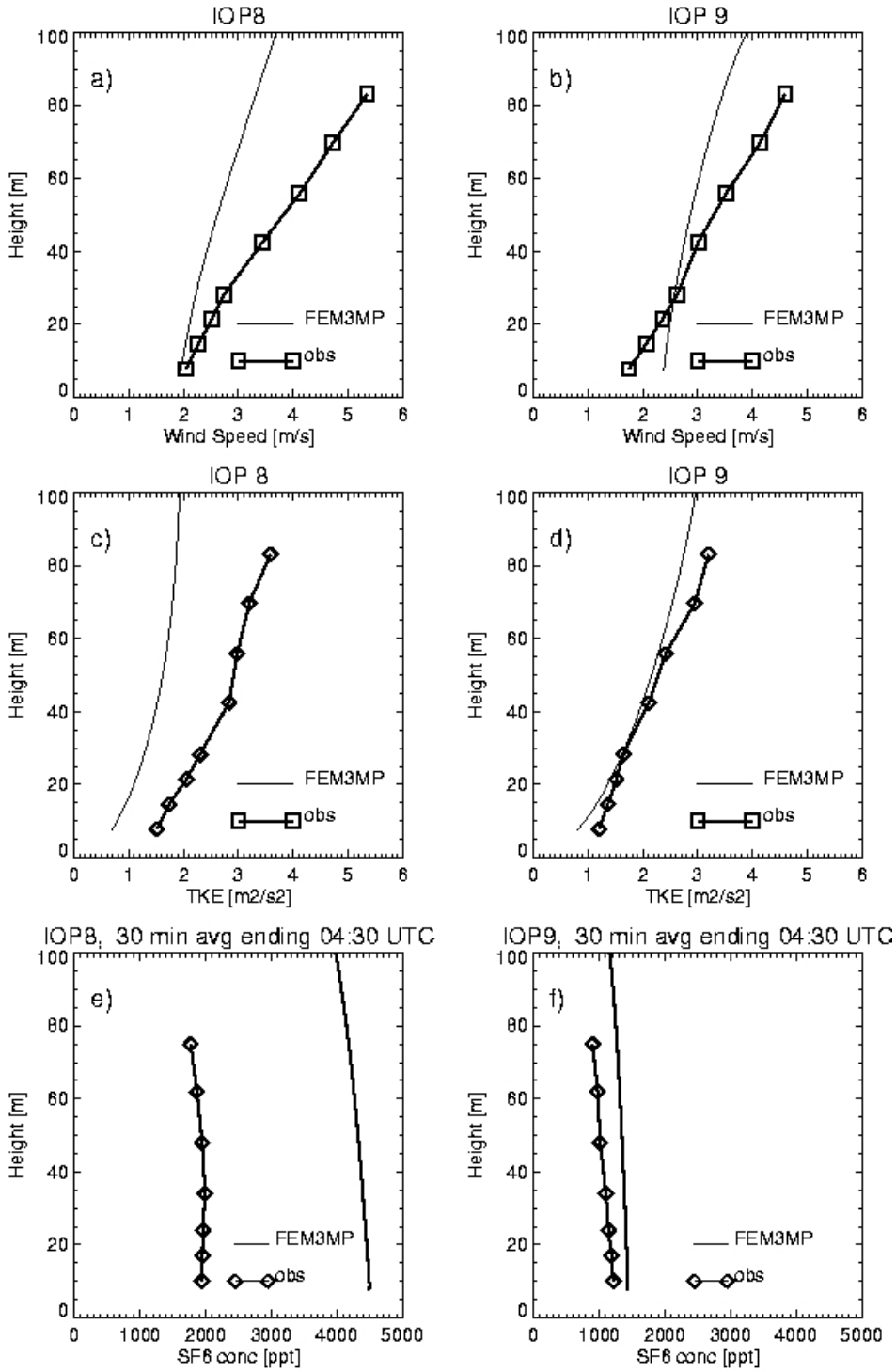

Figure 4: Comparison of CFD results at the crane location to observations: a) velocity profile for IOP8, b) velocity profile for IOP9, c) TKE profile for IOP8, d) TKE profile for IOP9, e) SF6 concentration profile for IOP8, f) SF6 concentration profile for IOP9. Note the good agreement for IOP9 (b,d,f) and the poor agreement for IOP8 (a,c,e).

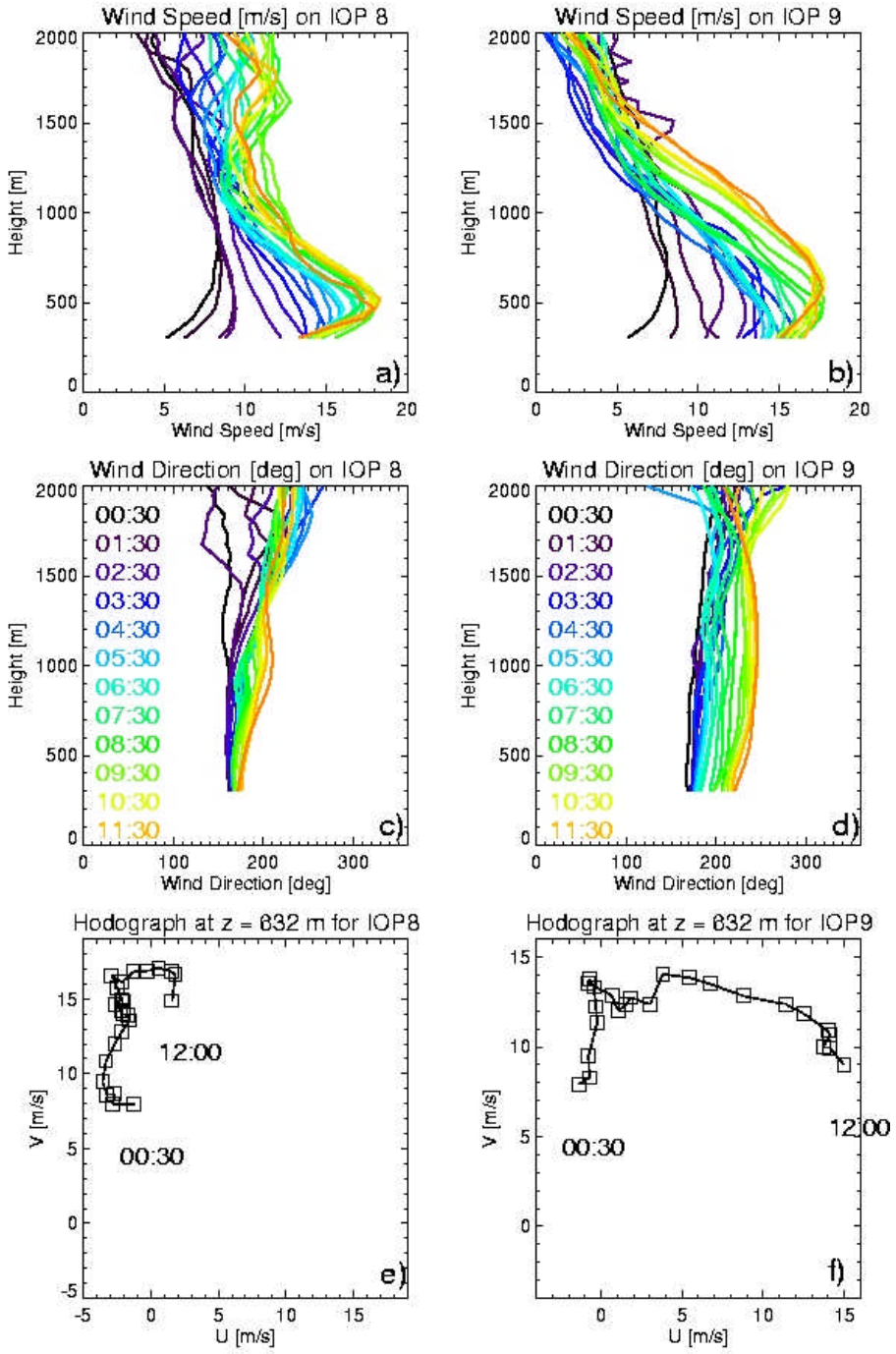

Figure 5: The evolution of wind profiles every 30 minutes from 0030 UTC (black) to 1200 UTC (orange) on the nights of IOP8 (a,c,e) and IOP9 (b,d,f): a) wind speed for IOP8, b) wind speed for IOP9, c) wind direction for IOP8, d) wind direction for IOP9, e) hodograph from 630m level for IOP8, f) hodograph from 630m for IOP 9.

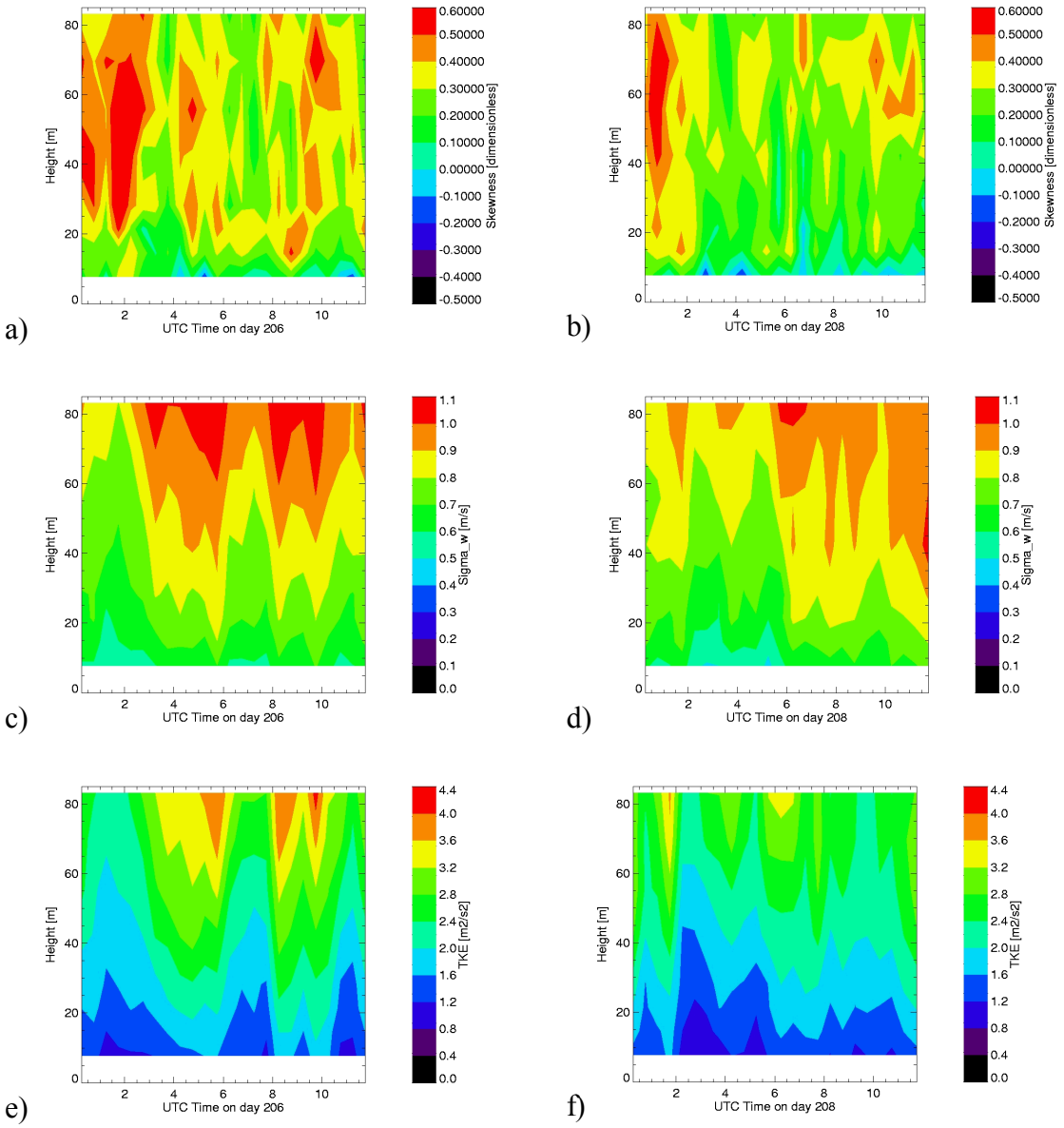

Figure 6: Time-height cross-sections from 0000 UTC to 1200 UTC on the nights of IOP8 (left panels a, c, e) and IOP9 (right panels b, d, f): a) skewness during IOP8, b) skewness during IOP9, c) σ_w, the standard deviation of vertical velocity during IOP8, d) σ_w, the standard deviation of vertical velocity during IOP9, e) TKE during IOP8, f) TKE during IOP9.

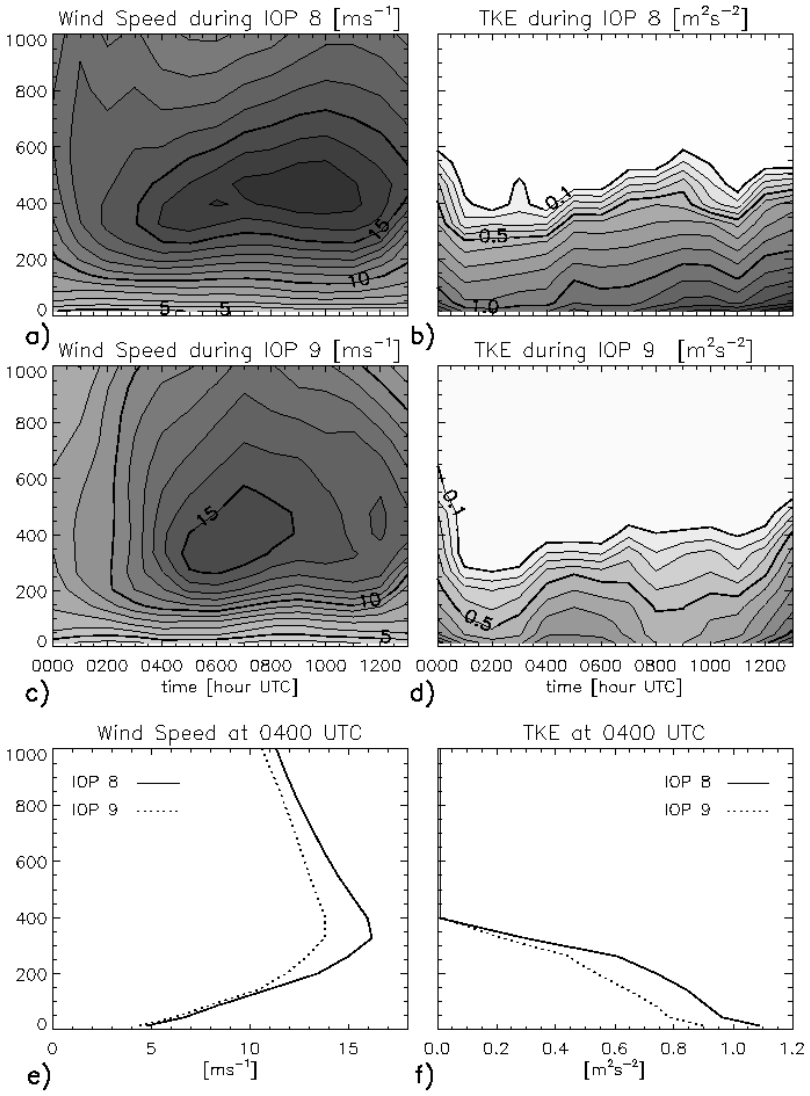

Figure 7: WRF simulations of the nights of IOPs 8 and 9. a) Time-height cross section of wind speed in the lowest 1000m from 0000 UTC to 1300 UTC on the night of IOP8. b) Time-height cross-section of turbulent kinetic energy in the lowest 1000m from 0000 UTC to 1300 UTC on the night of IOP8. c) As in a), but for IOP9. d) As in b), but for IOP9. e) Profiles of wind speed at the time of the CFD simulations, showing that the wind speed maximum for IOP 8 exceeds that of IOP9. f) Profiles of simulated TKE at the time of the CFD simulations, showing higher levels of TKE for IOP8 than for IOP9, but much smaller than observed or simulated by FEM3MP.